Poincaré-sphere representation of phase-mostly twisted nematic liquid crystal spatial light modulators

V Durán,[1] P Clemente,[2] Ll Martínez-León,[1] V Climent, [1] and J Lancis[1]

[1]GROC·UJI, Departament de Física, Universitat Jaume I, E12071 Castelló, Spain

[2]Servei Central d'Instrumentació Científica, Universitat Jaume I, E12071 Castelló, Spain

E-mail: *vduran@sg.uji.es*

Abstract

We establish necessary conditions in order to design a phase-only wave front modulation system from a liquid crystal display. These conditions determine the dependence of the polarization state of the light emerging from the display on the addressing gray level. The analysis, which is carried out by means of the coherence-matrix formalism, includes the depolarization properties of the device. Two different types of polarization distributions at the output of the liquid crystal cells are found. This approach is applied to a twisted nematic liquid crystal display. In this case, an optimization algorithm must be designed in order to select the input polarization state that leads to the required distributions. We show that the Poincaré-sphere representation provides a convenient framework to design the optimization algorithm as it allows for a reduced number of degrees of freedom. This feature significantly decreases the computation time. Laboratory results are presented for a liquid crystal-on-silicon display showing a phase modulation depth greater than 2π radians with an intensity variation lower than 6%. In addition, a hybrid-ternary modulation (HTM), an operation regime employed in holographic data storage, is achieved.

Keywords: liquid crystal devices, Poincaré sphere, phase modulation, polarization

PACS: 42.79.Kr Display devices, liquid-crystal devices, 42.25.Ja Polarization

1. Introduction

Off-the-shelf twisted nematic liquid crystal displays (TNLCDs) are subjected to a sustained performance improvement in order to attend the needs of the projection industry. TNLCDs based on liquid crystal on silicon (LCoS) technology are currently characterized by a high spatial resolution (10-μm pixel-pitch) and an excellent fill factor (>90%) [1]. For this reason, the optimization of commercial TNLCDs as spatial light modulators (SLMs) in non-display applications has kept a considerable interest in the last two decades [2-7]. Since TNLCDs are polarization-sensitive devices, such an optimization consists in their integration in a suitable polarimetric arrangement, which includes a polarization state generator (PSG) formed by a linear polarizer and a retardation plate, and a polarization state analyzer (PSA) consisting of identical elements but in reversed order.

The optimization of a TNLCD requires, as a previous step, a complete polarimetric characterization of liquid crystal (LC) cells as a function of the applied voltage. This calibration process can be performed by measuring the LC Jones matrices [8] or, in the context of the so-called retarder-rotator approach, the LC characteristic parameters [9]. If the display shows a significant depolarization effect, it is convenient to use the Stokes-Mueller matrix formalism instead of the Jones matrix calculus [10]. In this case, the TNLCD polarization properties can be extracted from experimental Mueller matrices with the aid of the polar decomposition [11].

In many applications, the goal of SLMs is to achieve a spatial control of the phase of an input wavefront without intensity variations. It is known that the electrically controlled birefringence of a LC cell yields a phase retardation effect. In the case of reflective TNLCDs, as widely used liquid crystal on silicon (LCoS) displays, the double pass of light through the medium produces a phase modulation depth of at least 2π at visible wavelengths. However, a twisted nematic structure inherently causes a voltage-dependent change of the state of polarization (SOP) of an input light beam [12]. This SOP modulation not only modifies the TNLCD phase response but can also produce intensity variations at the output of the PSA. Different methods have been proposed to overcome the SOP modulation due to the twisted nematic

alignment, with the use of the elliptically polarized eigenstates of a TNLCD standing out [4,5]. However, a significant variation of these eigenstates along the dynamic range of the display constitutes a major drawback of such procedure.

A frequently adopted approach for optimizing the phase response of a TNLCD is to perform a numerical simulation for searching the configurations of the PSG and the PSA that lead to the desired operation curve [8]. The amplitude and phase of the output electric field are determined with the aid of the Jones matrix calculus, which can also be combined with the Mueller matrix formalism if the display exhibits a non negligible depolarization effect [11]. In such an optimization process, the optical system is considered a “black box” with certain degrees of freedom, whose number is fixed by the particular election of the elements integrating the PSG and the PSA. The final configuration is obtained from an algorithm that optimizes a merit function, defined to ensure a flat intensity response with the largest phase modulation depth. This merit function usually depends on a considerable number of variables, leading to cumbersome and time-consuming calculations.

In this paper we point out the necessary condition for the SOP modulation provided by a LC display that works as a continuous phase-only SLM. With the aid of the coherence-matrix formalism [13], we recognize that the SOP of the light impinging onto the PSA must show, as the voltage addressed to the display is changed, a well-defined distribution in the Stokes-parameter space. Discarding depolarization effects, there are merely two possibilities: 1) the SOP is distributed along any circumference on the Poincaré sphere normal to the transmission axis of the analyzer, or 2) the SOP remains unaltered, i.e., it is represented by a single representative point in the Stokes-parameter space for all the voltages. Previously reported phase-only modulation schemes for a TNLCD are classified into one of these two categories. That is the case of the two configurations analyzed in Ref. [14], each corresponding to one of the above SOP distributions, which are compared by means of a phasor analysis of polarization eigenvectors generated in a transmissive TNLCD.

The restrictions on the Stokes parameters for obtaining the desired distributions at the output of a LC-SLM dramatically reduce the number of possible angular configurations of the PSG. Once the

configuration of the PSG is fixed, the PSA only admits certain orientations for which the intensity modulation is negligible. In this way a set of feasible angular configurations for the polarimetric system is selected. The optimization is completed through the choice of the configuration that produces the maximum phase modulation depth. This step is performed with the aid of the Jones matrix calculus. The above analysis of the SOP modulation is also extended to the case of a display showing a non-negligible depolarization effect.

[The experimental work is conducted with an LCoS display. The light impinging onto the LC cells is elliptically polarized and the beam emerging from the display is analyzed with a single linear polarizer, which constitutes a simpler election for the PSA than that usually employed. As stated previously, two kinds of SOP distributions must be imposed at the output of the TNLCD. Both possibilities are considered for the sample display. For the former type, we have found an optimal configuration that produces a phase modulation depth higher than 2π rad. (at 633 nm) with intensity variations lower than 6 %. In the latter configuration, where the SOP is restrained to undergo a minimal variation, the phase-mostly modulation response is achieved in a limited part of display dynamic range, but with a higher intensity transmission level. In this case, a straightforward reorientation of the output polarizer leads to the so-called hybrid ternary modulation (HTM) regime. In the HTM regime, which has been used for holographic data storage [15,16], the TNLCD works only with three levels: a dark level with null transmission and two white levels of equal intensity and with a phase difference of 180º. In all preceding configurations, experimental operation curves for the sample TNLCD are presented and discussed].

As was mentioned above, the optical system consisting of a TNLCD and several polarization components was usually considered a sort of black box, and the algorithm to find the suitable polarization distributions was a blind process, as is reported in Ref. [8,11,20]. In these works, a numerical solution was reached from a merit function that depends on several variables, without deeper comprehension of the physics behind that solution. The presented approach offers meaningful understanding about the changes of polarization in a TNLCD-based system thanks to a Poincaré-sphere representation. The

corresponding optimization algorithm provides a reduced computation time, as will be shown in the discussion of the experimental results. On the other hand, a comprehensive exploration of the phase-only modulation capabilities of a TNLCD is achieved for any choice of the elements integrating the PSG and the PSA. To prove this point, a simplified architecture for the PSA, which just includes a single linear polarizer, is selected. With this polarization arrangement, it is not only possible to achieve a phase response similar to that previously reported in Ref. [11], but also to find other interesting operation regimes, as the so-called hybrid ternary modulation (HTM) regime. This operation regime has been used for holographic data storage [15,16]. In this way, the potential of our scheme is broadened to a more diversified scope, including LC systems that can potentially be subjected to depolarization effects. Moreover, the reported approach is a general method, valid for any kind of LC-based display working in a transmission or in a reflection mode. The procedures reported in Ref. [6,7] are particular cases of the general procedure demonstrated here.

2. Analysis of the SOP modulation provided by a phase-only LC-SLM

Let us consider a LC-SLM sandwiched between a PSG and a PSA, and illuminated with a laser light beam. We assume that the PSG and the PSA are nondepolarizing devices and any light depolarization effect is only due to the modulator. For such a polarimetric system, the SOP generated by the PSG is transformed, under the action of the LC-SLM, into a voltage-dependent SOP, which is projected by the PSA onto a single final polarization state. We deal with partially polarized light in the context of the coherence matrix formalism. Here, a SOP is described by the 2×2 complex hermitian matrix $\mathbf{\Phi}$ [13]

$$\mathbf{\Phi} \equiv \left\langle \mathbf{E}(t) \otimes \mathbf{E}^{+}(t) \right\rangle = \begin{pmatrix} \left\langle E_x(t) E_x^*(t) \right\rangle & \left\langle E_x(t) E_y^*(t) \right\rangle \\ \left\langle E_y(t) E_x^*(t) \right\rangle & \left\langle E_y(t) E_y^*(t) \right\rangle \end{pmatrix} = \begin{pmatrix} \Phi_{xx} & \Phi_{xy} \\ \Phi_{yx} & \Phi_{yy} \end{pmatrix}, \tag{1}$$

where $\otimes$ denotes the direct product of the instantaneous Jones vector $\mathbf{E}(t)$ and its transposed conjugated $\mathbf{E}^{+}(t)$; E_j ($j = x, y$) are the Cartesian components of the electric field; E_j^* stands for the complex conjugate of E_j, and the brackets indicate time averaging over the measurement time. Therefore, the LC-SLM

performs the transformation $\mathbf{\Phi}_1 \rightarrow \mathbf{\Phi}_2$, where $\mathbf{\Phi}_1$ and $\mathbf{\Phi}_2$ are, respectively, the coherence matrices corresponding to the light before and after the modulator. The input matrix $\mathbf{\Phi}_1$ is a single state that depends on the configuration of the PSG. The output matrix $\mathbf{\Phi}_2$ is a function of the parameter g that controls the voltage applied to the LC cells. Hence, the LC-SLM actually behaves as a SOP modulator.

In order to analyze the effect of the PSA over each SOP generated by the LC-SLM, it is convenient to express $\mathbf{\Phi}_2$ (for any value of g) as a linear expansion of the Pauli matrices $\boldsymbol{\sigma}_j$, [13]

$$\mathbf{\Phi}_2 = \frac{1}{2}\sum_{j=0}^{3} S_j \boldsymbol{\sigma}_j = \frac{1}{2}\begin{pmatrix} S_0 + S_1 & S_2 - iS_3 \\ S_2 + iS_3 & S_0 - S_1 \end{pmatrix}, \tag{2}$$

where the matrices $\boldsymbol{\sigma}_j$ are given by

$$\boldsymbol{\sigma}_0 = \begin{pmatrix} 1 & 0 \\ 0 & 1 \end{pmatrix}, \quad \boldsymbol{\sigma}_1 = \begin{pmatrix} 1 & 0 \\ 0 & -1 \end{pmatrix}, \quad \boldsymbol{\sigma}_2 = \begin{pmatrix} 0 & 1 \\ 1 & 0 \end{pmatrix}, \quad \boldsymbol{\sigma}_3 = \begin{pmatrix} 0 & -i \\ i & 0 \end{pmatrix}, \tag{3}$$

i is the imaginary unit and S_j (j = 0, 1, 2, 3) are the Stokes parameters of the light after the LC-SLM. These parameters can be obtained from the trace of the coherence matrix $\mathbf{\Phi}_2$ as

$$S_j = tr(\mathbf{\Phi}_2 \sigma_j) \quad j \in [0, 3]. \tag{4}$$

From this equation, $S_0 = tr(\mathbf{\Phi}_2)$ is the total intensity of the light beam impinging onto the PSA. The normalized version of the coherence matrix $\mathbf{\Phi}_2$ is the density matrix $\mathbf{D}_2$,

$$\mathbf{D}_2 \equiv \frac{\mathbf{\Phi}_2}{tr(\mathbf{\Phi}_2)} = \frac{1}{2}\begin{pmatrix} 1 + s_1 & s_2 + is_3 \\ s_2 - is_3 & 1 - s_1 \end{pmatrix}, \tag{5}$$

where $s_j \equiv S_j / S_0$. Note that the density matrix remains entirely determined by the normalized parameters s_j, which can be arranged in a 3×1 Stokes vector $\mathbf{P}$, $\mathbf{P} = (s_1, s_2, s_3)^T$, with T indicating the transposed vector. The fraction of the intensity emerging from the LC-SLM that is detected after the PSA, I, is given by [17]

$$I = Tr(\mathbf{D}_A \mathbf{D}_2) \ , \tag{6}$$

where $\mathbf{D}_A$ is the density matrix constructed using the 3×1 Stokes vector **Q** corresponding to the fully transmitted eigenstate of the PSA. In general, this eigenstate is elliptically polarized. From Eqs (5) and (6), we have

$$I = \frac{1}{2}(1 + \mathbf{P} \cdot \mathbf{Q}) . \tag{7}$$

This expression admits a geometrical interpretation if we map the vectors **P** and **Q** in the Poincaré-sphere representation, as is shown in figure 1. By taking into account that the vector **Q** corresponding to transmission axis of the PSA has a unit modulus, we achieve

$$I = \frac{1}{2}(1 + \rho \cos\theta) , \tag{8}$$

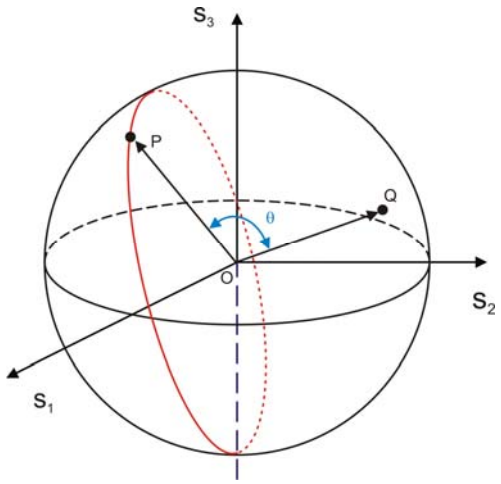

Figure 1: a) Action of an elliptical polarizer over an arbitrary SOP in the Poincaré sphere representation. The radius vectors OQ and OP represent, respectively, the orientation of the polarizer transmission axis and the input SOP. The red circle corresponds to a distribution of *type I* that leads to a flat intensity response at the output of the polarizer.

where $\rho = |\mathbf{P}|$ is the degree of polarization (DOP) of the light emerging from the LC-SLM. If the modulator does not produce any depolarization effect, $\rho = 1$, the endpoints of **P** and **Q** are on the surface of the Poincaré sphere of unit radius and Eq. (8) is reduced to $I = \cos^2(\theta/2)$. In this way, we retrieve the

well-established rule stating that the fraction of the input intensity transmitted by an arbitrary polarizer is equal to the square cosine of half the angle θ between the unit vectors that represent, respectively, the input SOP and the polarizer transmission axis [18].

In light of the above geometrical approach, let us analyze the SOP modulation provided by a phase-only LC-SLM. In the absence of depolarization, the states described by the matrices $\mathbf{\Phi}_2(g)$ trace out a trajectory on the surface of the Poincaré sphere as the value of g is changed. As the intensity transmitted by the PSA must remain constant, there are only two possibilities, leading to two types of distributions:

Type I. The trajectory on the sphere corresponds to an arbitrary circumference and the transmission axis of the PSA is oriented normal to the plane containing the set of SOPs, as is shown in figure 1. Such a polarization distribution ensures a constant value of I, since the angle θ remains unaltered along the dynamic range of the modulator. The generation of equi-azimuth polarization states, described in Ref. [6], is a particular case of this type of SOP modulation.

Type II. The SOP distribution at the output of the LC-SLM is reduced to the trivial case of a single point for all values of g, which means that there is not a SOP modulation. The orientation of the PSA is, in principle, arbitrary. However, it is convenient to choose an angle for the analyzer axis that leads to a maximum level of transmitted intensity.

If the light impinging onto the PSA is partially polarized by the action of the LC-SLM, an extra condition must be added. Now, the intensity contribution also depends on the DOP of the impinging light. Hence, a phase-only modulation response requires a constant DOP along the modulator dynamic range in order to avoid residual intensity variations. In the Stokes parameter space, this means that the points of the SOP distribution generated by the LC-SLM must remain on the same spherical surface with a radius equal to the DOP of the light. Although a constant DOP is the main requisite for a phase-only operation, it is also desirable to reduce the unpolarized component in order to avoid non-controllable background light at the output of the system.

The above SOP distributions are only approximately achieved by TNLCDs. Hence, we can obtain, in the best-case scenario, a phase-mostly modulation response with this kind of modulators. SOP distributions close to the two types of a phase-only LC-SLM will be also denoted as distributions of *Type I* or *Type II*.

We note that it is also possible to remove the PSA to preserve a constant light intensity at the output of the system. Without any output polarizer, the polarization modulation provided by the LC-SLM cannot be traduced in an intensity modulation. This configuration has been recently used for the design of advanced algorithms for the reconstruction of digital or computer-generated holograms [19]. However, if that situation is desired, the scalar diffraction theory could not longer be used. The apparent simplicity of the system would, in contrast, involve a more complex analysis, and the use of Jones Calculus would be required in the beam propagation algorithm.

3. Calibration of the TNLCD

For the sake of completeness, we review the polarimetric characterization of a TNLCD. A detailed analysis can be found in Ref. [11]. The calibration is performed through the measurement of the Mueller matrices, $\mathbf{M}_{\mathrm{TNLCD}}(g)$, of the display for each value of the parameter g. Neglecting diattenuation effects, the matrix elements of $\mathbf{M}_{\mathrm{TNLCD}}(g)$ are measured by the generation of four different SOPs, represented by the Stokes vectors $\mathbf{S}_i$ (i = 1,...,4), corresponding to horizontal, vertical and 45º linearly polarized light, and right-handed circularly polarized light, respectively. In this way, we construct a 4×4 matrix $\mathbf{N}_1$, whose columns are the input vectors $\mathbf{S}_i$. Afterwards, the corresponding Stokes parameters for the light emerging from the display $\mathbf{S}_i$'(g) are measured. For each value of the gray level, these vectors, arranged in columns, determine a second 4×4 matrix $\mathbf{N}_2$ (g). Taking into account that $\mathbf{N}_2(\mathrm{g}) = \mathbf{M}_{\mathrm{TNLCD}}(g)\ \mathbf{N}_1$, the Mueller matrices $\mathbf{M}_{\mathrm{TNLCD}}(g)$ are obtained as $\mathbf{M}_{\mathrm{TNLCD}}(g) = \mathbf{N}_2(g)\ \mathbf{N}_1^{-1}$.

It is also convenient to recall that the action of a TNLCD can be mimicked through a pure depolarizer and a pure retarder [11]. In mathematical terms,

$$\mathbf{M}_{\mathrm{TNLCD}} = \mathbf{M}_{\Delta}\,\mathbf{M}_{R}\,, \tag{9}$$

where $\mathbf{M}_{\Delta}$ and $\mathbf{M}_{R}$ are, respectively, the Mueller matrices corresponding to the depolarizer and the retarder. Note that once the experimental Mueller matrices $\mathbf{M}_{\mathrm{TNLCD}}(g)$ are measured, the non-depolarizing response of the display as a function of g can be assessed by use of the Lu-Chipman decomposition technique. This approach allows for a simple evaluation of the phase modulation due to the display cells [11,20].

4. Optimization of the TNLCD phase response

4.1. Flat intensity response

Let us consider a TNLCD sandwiched between a PSG, formed by a linear polarizer and a quarter-wave plate, and a PSA, constituted by a single linear polarizer. The transmission axis of the first polarizer and the fast axis of the quarter wave plate are oriented, respectively, at angles ζ_1 and ξ_1 from the horizontal direction of the laboratory framework. The analogous angle for the polarizer of the PSA is denoted by ζ_2. In order to ensure a flat intensity response after the PSA, we search the configuration of the PSG that approximately produce the SOP distributions described in Sec. 2 at the output of the TNLCD. In practice, there is not a single solution for the SOP impinging onto the display, but the number of possible values of the angles (ζ_1, ξ_1) is limited.

The 4×1 Stokes vector of the totally polarized light impinging onto the TNLCD, **S**, is

$$\mathbf{S}(\zeta_1,\xi_1) = \begin{pmatrix} 1 \\ \cos 2\xi_1 \cos 2(\xi_1-\zeta_1) \\ \sin 2\xi_1 \cos 2(\xi_1-\zeta_1) \\ \sin 2(\xi_1-\zeta_1) \end{pmatrix}. \tag{10}$$

In the Stokes-Mueller formalism, the SOP corresponding to the light emerging from the display, **S'**, is given by

$$\mathbf{S}'(\zeta_1,\xi_1,g) = \mathbf{M}_{\mathrm{TNLCD}}(g)\,\mathbf{S}(\zeta_1,\xi_1)\,. \tag{11}$$

The output vector has the form $\mathbf{S}'(\zeta_1, \xi_1, g) = (1, s_1', s_2', s_3')^T$, where $s_i'(\zeta_1, \xi_1, g)$ are the normalized Stokes parameters $s_i' = S_i'/S_0'$ (i=1, 2, 3). The Stokes vector $\mathbf{S}_f(\zeta_1, \xi_1, \zeta_2, g)$ after the analyzer is

$$\mathbf{S}_f(\zeta_1, \xi_1, \zeta_2, g) = \mathbf{M}_P(\zeta_2)\mathbf{S}'(\zeta_1, \xi_1, g), \tag{12}$$

where $\mathbf{M}_P$ is the conventional Mueller matrix for a linear polarizer [11]. The vector $\mathbf{S}_f(\zeta_1, \xi_1, \zeta_2, g)$, written in the analyzer framework, has the form $(I, s_{f1}, s_{f2}, 0)$ and corresponds to a linear SOP with an intensity $I(\zeta_1, \xi_1, \zeta_2, g)$. Note that, in general, the optimization procedure to achieve a flat intensity response deals with three angular parameters that must be varied within the angular range for the polarizing devices.

A simplified search algorithm is derived with the aid of the calculations presented in Section 2. To this end, let us search the values of the parameters (ζ_1, ξ_1) that lead to a polarization distribution of *Type I*. Note that only two parameters for the search algorithm remain. Here, the SOPs at the output of the TNLCD are approximately located in a circumference on the Poincaré sphere and the transmission axis of the PSA is normal to the plane containing this circumference. We assume a linear polarizer for the PSA. In this case, the transmission axis is represented by a radius vector whose endpoint is in the Equator of the Poincaré sphere. Consequently, the set of SOPs at the output of the TNLCD must be located in a circle orthogonal to the equator, as is shown in figure 2, so they trace out a straight line in the $S_1 - S_2$ plane. In other words, a linear correlation between the parameters s_1' and s_2' must exist. This means that the Pearson correlation coefficient $r(\zeta_1, \xi_1)$, conventionally used in linear regressions and defined as [21]

$$r = \frac{N\sum_g s_1's_2' - \sum_g s_1' \sum_g s_2'}{\sqrt{N\sum_g (s_1')^2 - \left(\sum_g s_1'\right)^2}\sqrt{N\sum_g (s_2')^2 - \left(\sum_g s_2'\right)^2}}, \tag{13}$$

must be close to the unity. In Eq. (13), *N* is the number of values taken by the parameter *g* along the pixel dynamic range and, for the sake of clarity, the angular dependence of the magnitudes has been removed. We use this parameter as the merit function for the search algorithm.

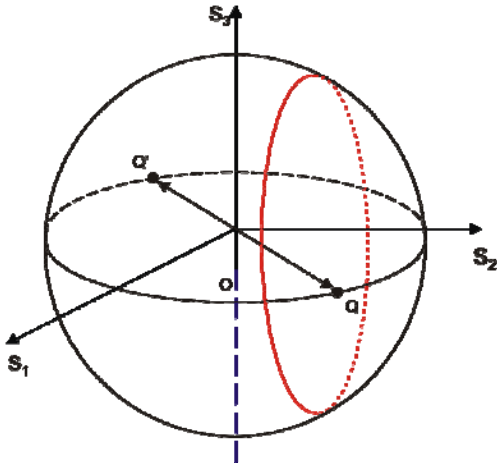

Figure 2. Distribution of *type I* when the PSA is constituted by a linear polarizer. The two possible orientations for the polarizer, corresponding to mutually orthogonal directions, are represented by the same line, which intersects the sphere equator in the antipodal points Q and Q'.

Once an angular configuration for the PSG is selected, the transmission axis of the analyzer only admits two orientations corresponding to mutually orthogonal directions, which are represented in the Poincaré sphere by the same straight line, as depicted in Fig1b. Note that the above reasoning can be easily extended to the case of a PSA formed by a linear retarder and a linear polarizer. In such a situation, the PSA is an elliptical analyzer and its transmission can be arbitrarily oriented in the Stokes space. This means that the set of SOPs after the TNLCD are in general located in a circumference that is no longer normal to the Equator (this general situation is shown in Fig1a). However, there must be a linear relation between s_1', s_2' and s_3', as the SOPs are contained in the same plane. Now, we can use the correlation coefficient of the corresponding multiple regression to determine the optimal values for ζ_1 and ξ_1.

If the display produces a significant depolarization effect, we must include in the search algorithm an additional step concerning the degree of polarization, DOP(ζ_1, ξ_1, g),

$$\mathrm{DOP} = \sqrt{(s_1')^2 + (s_2')^2 + (s_3')^2}\ , \tag{14}$$

and demand a constant (and maximum) value for this parameter.

In the case of the polarization distributions of *type II*, each of the normalized Stokes parameters $s_i'(\zeta_1, \xi_1, g)$ must undergo a minimal variation along the pixel dynamic range. We can find the optimal PSG configuration by minimizing the function $F(\zeta_1, \xi_1)$,

$$F = \sum_{i=1}^{3} \sigma_i\ , \tag{15}$$

where σ_i (i=1, 2, 3) are, respectively, the standard deviations of the corresponding Stokes parameters $s_i'(\zeta_1, \xi_1, g)$ for the N values taken by the parameter g. Note that the minimization of the function F also ensures a constant degree of polarization. Concerning the PSA, its angular configuration is chosen with the aim of achieving a maximum transmitted intensity level.

4.2. Phase response maximization

The optimization algorithm provides a limited number of angular configurations for the PSG and the PSA that ensure a flat intensity response. Now, we must select from the above set the configuration that yields a maximum phase modulation depth. To this end, we evaluate the phase of the light field through the Jones vector $\mathbf{E}_f$ corresponding to the light emerging from the PSA. In this way,

$$\mathbf{E}_f(\zeta_1, \xi_1, \zeta_2, g) = \mathbf{J}_{\mathrm{PSA}}(\zeta_2)\, \mathbf{J}_{\mathrm{TNLCD}}(g)\, \mathbf{E}_{\mathrm{PSG}}(\zeta_1, \xi_1)\ , \tag{16}$$

where $\mathbf{E}_{\mathrm{PSG}}$ is the Jones vector of the SOP determined by Eq. (10), $\mathbf{J}_{\mathrm{TNLCD}}(g)$ is the Jones matrix describing the nondepolarizing effect of the display and $\mathbf{J}_{\mathrm{PSA}}$ is the Jones matrix of the linear polarizer that constitutes the PSA of the system. The electric field of Eq. (16), written in the final polarizer framework, has the form $\mathbf{E}_f = \exp[-i\,\phi(\zeta_1, \xi_1, \zeta_2, g)]\, A\, (1 \quad 0)^T$, i.e., corresponds to linearly polarized

light with a real amplitude A and a global phase factor $\exp(-i\phi)$, which depends on the value taken by the parameter g as well as on the angular configuration of the system [6,11]. The optimization algorithm is completed by selecting the combination (ζ_1, ξ_1, ζ_2) that produce the maximum variation of ϕ along the pixel dynamic range.

5. Experimental results

The laboratory set-up used for optimizing the phase response of a TNLCD is shown in figure 3. The illumination system consists of a He-Ne laser (LS) emitting at 633 nm, a spatial filter SF and a collimating lens L_1. The polarization state generator (PSG) comprises a linear polarizer P_1 followed by a zero-order quarter-wave plate QWP designed for 633 nm. The TNLCD is a reflective LCoS display, an Aurora panel, model ASI 2000, with XGA resolution (1024×768 pixels), designed for red light and commercialized by Holoeye. The TNLC cells have a twist angle of 45º and the pixel array has a period of 19 μm with an inactive gap of 1μm. The application of a voltage to the pixels is performed by displaying

a gray-level image, so the parameter g is here the addressed gray-level. Note that the direction of incidence of the light beam impinging onto the LCoS display is not normal in order to avoid the use of nonpolarizing beam-splitters, which present some non negligible retardance and diattenuation effects [10]. The angular separation of the input and output beams is very small ($\alpha = 4^{\circ}$) so the validity of Mueller matrix formalism is preserved.

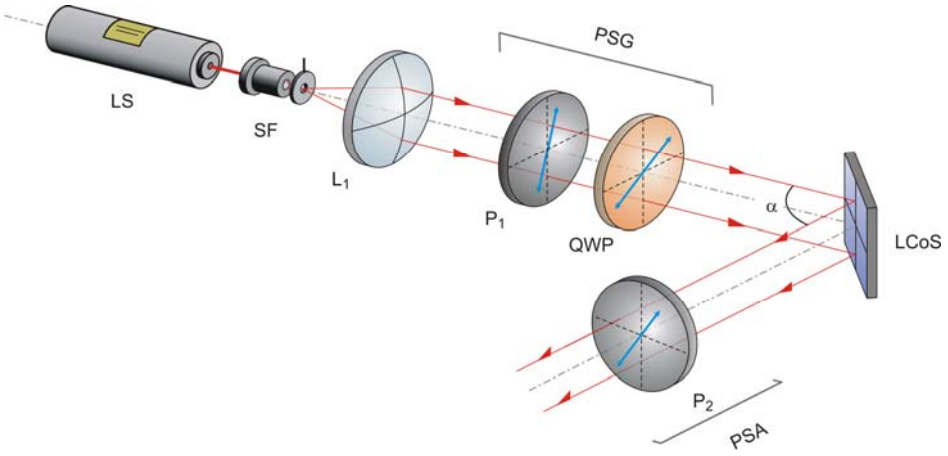

Figure 3. Optical set-up for optimizing the phase response of an LCoS display (angle not to scale).

We have applied the optimization procedure described in the preceding sections to the sample display. First, the matrix $\mathbf{M}_{\mathrm{TNLCD}}(g)$ for the TNLCD was experimentally determined using the calibration method outlined in Section 3. The Stokes parameters $s_i'(\zeta_1, \xi_1, g)$ after the LC cells were calculated varying the angles (ζ_1, ξ_1) of the polarization elements in the PSG in steps of 1º. The Pearson correlation coefficient $r(\zeta_1, \xi_1)$ and the standard deviations $\sigma_i(\zeta_1, \xi_1)$ corresponding to Eq. (13) and (15) were valuated by means of conventional calculus software. The above merit functions provide a reduced set of angular configurations that satisfy the search criterion. The orientation of the polarizer in the PSA, ζ_2, is then fully determined from the values of (ζ_1, ξ_1). For the SOP of type II, the polarizer in the PSA is oriented to achieve a maximum intensity transmittance. After the angular configuration for the elements in the PSG and the PSA is determined, we evaluate the phase function $\phi(\zeta_1, \xi_1, \zeta_2, g)$ to select the configuration providing a maximum modulation depth.

After obtaining the optimal configurations, we have experimentally verified them. To this end, the transmitted intensity $I(\zeta_1, \xi_1, \zeta_2, g)$ at the output of the PSA and the phase function $\phi(\zeta_1, \xi_1, \zeta_2, g)$ were experimentally measured. In order to measure the LCoS phase modulation for the optimal configurations we use the fractional-Talbot effect [6,22]. With the LCoS display, we implement different

binary gratings where one gray level is fixed and the other is variable. We choose the gray level g = 255 as a reference, which for the sample display corresponds to a maximum applied voltage. The relative phase shift is determined by measuring the contrast of the Fresnel images at a quarter of the Talbot distance. Concerning the transmitted intensity $I(\zeta_1, \xi_1, \zeta_2, g)$, it was measured with the aid of a photometer by displaying uniform images for each gray level on the LCoS display.

For the polarization distribution of *type I*, the optimal phase response is achieved when ζ_1 = 74º, ξ_1 = 93º, and ζ_2 = 63º. The SOP distribution at the output of LC cells, obtained from Eq. (11), has been depicted on the Poincaré sphere in figure 4(a). By means of a least-squares procedure, the linear relation between S_1 and S_2 is found to be $S_2 = -0.06 + 0.70\,S_1$, with a correlation coefficient of $r = 0.95$. The circumference on the Poincaré sphere for which this relation holds is also shown in figure 4(a). The DOP has a mean value of 0.98 along the entire pixel dynamic range and a standard deviation of 2%. The mean value of the intensity transmitted by the analyzer, which can be calculated through Eq. (11), is of 46%, with a maximum variation of 11%. The measured intensity and phase curves for the optimal configuration are shown in figure 5. The phase modulation depth is greater than 2π radians and the output intensity level is around 43%, with a residual variation lower than 11%. These results show a well agreement with those obtained from theoretical calculations. If the points corresponding to g < 23 are removed, the maximum intensity variation is reduced to 6% preserving a maximum phase shift of 2π.

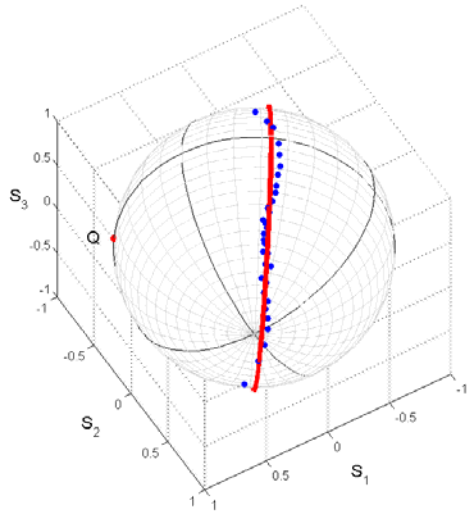

(a)

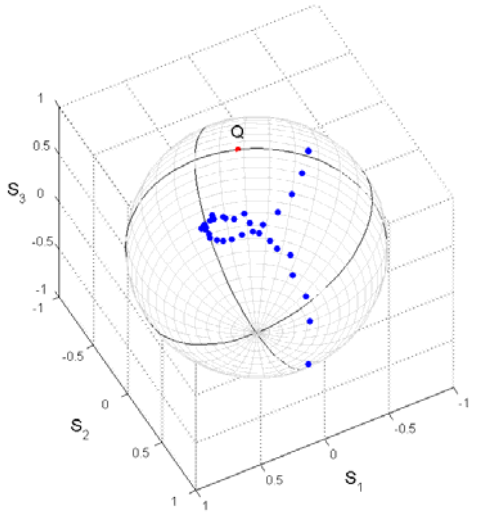

(b)

Figure 4: Poincaré-sphere representation of the SOPs at the output of the LCoS display for the optimal configuration corresponding to a) the SOP distribution of *type I* and b) the SOP distribution of *type II*.

Concerning the polarization distributions of *type II*, the optimal phase response is achieved for $\zeta_1 = 128^o$, $\xi_1 = 21^o$, and $\zeta_2 = 100^o$. The corresponding SOP distribution at the output of the LC cells is depicted in figure 4(b). The DOP remains again approximately constant with a mean value of 0.95 and a standard deviation of 2%. Note that the SOPs clearly trace out a loop-shaped trajectory on the Poincaré sphere. Hence, for the present LCoS display it is not possible to concentrate all representative points in a small region of the Stokes parameter space. However, a proper orientation of the output linear polarizer, $\zeta_2 = 100^o$, yields an almost flat intensity response for a considerable part of the pixel dynamic range. In this range, a highly efficient transmission close to 90% is obtained (a 100% transmission corresponds to the ideal situation where there is no polarization-dependent absorption by the action of the analyzer). Theoretical calculations from Eq. (12) show a mean intensity value of 88% for g <203, with a maximum variation of 8%. The measured intensity and phase response curves are represented in figure 6. For the aforementioned range, the mean intensity value is of 91 % with a maximum variation of 10%, which reasonably agree with the expected intensity response. The phase modulation depth is of about 1.3π radians.

The loop-shaped trajectory shown in figure 4(b) corresponding to $\zeta_1 = 128^o$ and $\xi_1 = 21^o$ can be used to obtain a hybrid ternary modulation. By setting the output linear polarizer at $\zeta_2 = 25^o$, the transmitted intensity for the points that intersect the equator of the sphere is very close to zero. In this way, we obtain the dark level of the HTM regime. The central part of the loop, on its turn, corresponds to SOPs that produce a smoothly intensity fluctuation after the PSA, as is shown in figure 7. This intensity curve is accompanied by a continuous phase modulation. This fact allows us to select two gray-level of equal transmission with a phase difference of π rad. For example, this situation is achieved for g = 83 and g = 223 with an intensity level of 18%. Despite the lack of efficiency, this configuration leads to similar results that those found in Ref. [16].

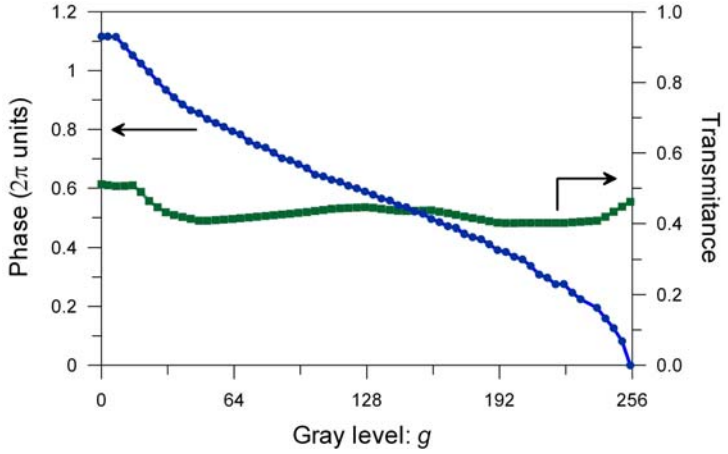

Figure 5: Intensity and phase modulation for the optimal configuration obtained from the SOP distribution of *type I*.

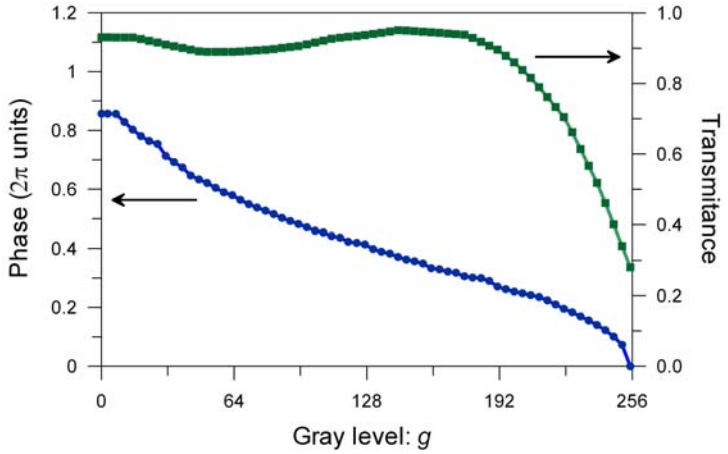

Figure 6: Intensity and phase modulation for the optimal configuration obtained from the SOP distribution of *type II*.

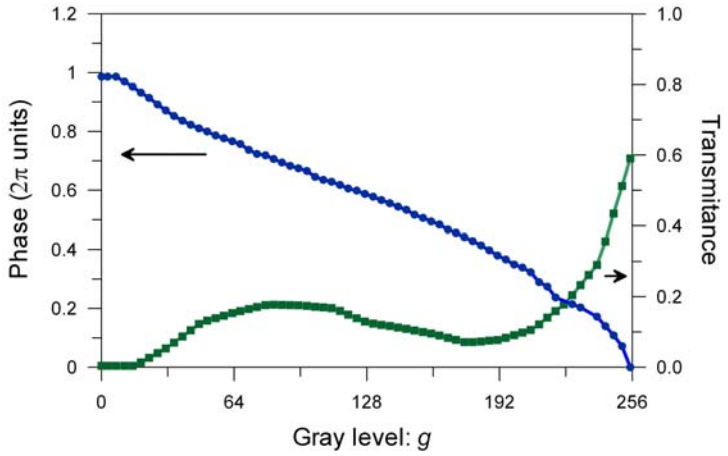

Figure 7: Intensity and phase modulation for the configuration that produces an HTM regime.

5. Discussion and conclusions

We have shown that a TNLCD acting as a phase-mostly SLM must provide a SOP modulation that is necessarily subjected to specific restrictions, which can be classified into two categories (*types I* and *II*). Such restrictions become a useful tool in the design of an efficient optimization algorithm, which leads to the election of suitable configurations for the polarimetric system where the SLM is integrated. A possible depolarization effect due to the TNLCD is also included in our analysis.

The presented approach enables a comprehensive exploration of the modulation capabilities of a sample display. Furthermore, it benefits from a noticeable reduction of the computation time. This point can be checked by comparing the search algorithm described in Sec.2 with that used in Ref. [11], where the sample display is sandwiched between two polarizers and two quarter-wave plates. By searching for a polarization distribution of *type I* and considering an elliptical analyzer, the computational time required to retrieve the optimal configuration of Ref. [11] is reduced in one order of magnitude (about 15 times) [Introduction of times].

In the present work, we have achieved a flat intensity response (with residual variations lower than 6%) and a phase modulation depth of 360º (at 633 nm) with a commercial LCoS display. We have used a simplified architecture for the PSA, which only includes a single linear polarizer. The use of this

PSA implies a reduction of computational complexity. Hence, it contributes to increase the algorithmic efficiency. We have found that the depolarization due to the sample display is a minor effect. However, for this kind of LCoS modulators the amount of depolarized light may be considerably larger at certain wavelengths and for certain input SOPs [23]. In such a case, the general approach presented in Sec. 2, which minimizes the effect of LCoS depolarization, results noticeably useful. In addition, our technique can be applied to other types of operation regimes, as for example the hybrid ternary modulation.

Acknowledgements

This research was funded by the Dirección General de Investigación Científica y Técnica, Spain, and FEDER under the project FIS2007-62217. Also partial funding from an agreement between the Universitat Jaume I and the Fundació Bancaixa-Caixa Castellón (project P1 1B2006-29) is acknowledged.

References

[1] Dai H T, Liu K X Y, Wang X and Liu J. H 2004 Characteristics of LCoS Phase-only spatial light modulator and its applications *Opt. Comm*. **238** 269-276

[2] Konforti N, Maron E and Wu S T 1988 Phase-only modulation with twisted nematic liquid-crystal spatial light modulators *Opt. Lett*. **13**, 251-253

[3] Lu K H and Saleh B E A 1990 Theory and design of the liquid-crystal TV as a spatial phase modulator *Opt. Eng*. **29**, 240-246

[4] Pezzaniti J L and Chipman R A 1993 Phase-Only Modulation of a Twisted Nematic Liquid-Crystal TV by Use of the Eigenpolarization States *Opt. Lett.* **18** 1567-1569

[5] Davis J A, Moreno I and Tsai P 1998 Polarization eigenstates for twisted-nematic liquid-crystal displays *Appl. Opt.* **37** 937-945

[6] Duran V, Lancis J, Tajahuerce E and Fernandez-Alonso M 2006 Phase-only modulation with a twisted nematic liquid crystal display by means of equi-azimuth polarization states *Opt. Express* **14** 5607-5616

[7] Duran V, Lancis J, Tajahuerce E and Climent V 2007 Poincaré Sphere Method for Optimizing the Phase Modulation Response of a Twisted Nematic Liquid Crystal Display *J. Displ. Technol.* **3**, 9-14

[8] Moreno I, Velasquez P, Fernandez-Pousa C R and Sanchez-Lopez M M 2003 Jones matrix method for predicting and optimizing the optical modulation properties of a liquid-crystal display *J. Appl. Phys.* **94**, 3697-3702

[9] Duran V, Lancis J, Tajahuerce E and Jaroszewicz Z 2006 Equivalent retarder-rotator approach to on-state twisted nematic liquid crystal displays 2006 *J. Appl. Phys*. **99** 113101-113106

[10] Wolfe J E and Chipman R A 2006 Polarimetric characterization of liquid-crystal-on-silicon panels *Appl. Opt.* **45** 1688-1703

[11] Clemente P, Duran V, Martínez-León Ll, Climent V, Tajahuerce E and Lancis J 2008 Use of polar decomposition of Mueller matrices for optimizing the phase response of a liquid-crystal-on-silicon display *Opt. Express* **16**, 1965-1974

[12] Gooch C H and Tarry H A 1975 Optical-Properties of Twisted Nematic Liquid-Crystal Structures with Twist Angles Less Than 90 Degrees *J. Phys. D-Appl. Phys.* **8** 1575-1584

[13] Brosseau C 1998 *Fundamentals of Polarized Light: a Statistical Optics Approach* (New York: John Wiley & Sons)

[14] Davis J A, Nicolás J and Márquez A 2002 Phasor analysis of eigenvectors generated in liquid-crystal displays *Appl. Opt.* **41** 4579-4584

[15] Jang J S and Shin D H 2001 Optical representation of binary data based on both intensity and phase modulation with a twisted-nematic liquid-crystal display for holographic digital data storage *Opt. Lett.* **26** 1797-1799

[16] Márquez A. Gallego S, Méndez D, Álvarez M L, Fernández E, Ortuño M, Neipp C, Beléndez A and Pascual I 2007 Accurate control of a liquid-crystal display to produce a homogenized Fourier transform for holographic memories *Opt. Lett.* **32** 2511-2513

[17] McMaster W H 1954 Polarization and the Stokes Parameters *Am. J. Phys.* **22** 351-362

[18] Jerrard H G 1954 Transmission of Light through Birefringent and Optically Active Media: the Poincaré Sphere *J. Opt. Soc. Am.* **44** 634-640

[19] Kohler C, Haist T, Schwab X and Osten W 2008 Hologram optimization for SLM-based reconstruction with regard to polarization effects *Opt. Express* **16** 14853-14861

[20] Moreno I, Lizana A, Campos J, Márquez A, Iemmi C and Yzuel M J 2008 Combined Mueller and Jones matrix method for the evaluation of the complex modulation in a liquid-crystal-on-silicon display *Opt. Lett.* **33** 627-629

[21] Bevington P R and Robinson D K 1992 *Data Reduction and Error Analysis for the Physical Sciences* 2nd ed. (New York: Mc Graw-Hill)

[22] Serrano-Heredia A, Lu G W, Purwosumarto P and Yu F T S 1996 Measurement of the phase modulation in liquid crystal television based on the fractional-Talbot effect *Opt. Eng.* **35**, 2680-2684

[23] Lizana A, Márquez A, Moreno I, Iemmi C, Campos J and. Yzuel M J 2008 Wavelength dependence of polarimetric and phase-shift characterization of a liquid crystal on silicon display *J. Eur. Opt. Soc* **3** 08012